

THE OFFICIAL MAGAZINE OF THE OCEANOGRAPHY SOCIETY

# Oceanography

## CITATION

Constantin, A., and R.S. Johnson. 2018. Steady large-scale ocean flows in spherical coordinates. *Oceanography* 31(3):42–50, <https://doi.org/10.5670/oceanog.2018.308>.

## DOI

<https://doi.org/10.5670/oceanog.2018.308>

## COPYRIGHT

This article has been published in *Oceanography*, Volume 31, Number 3, a quarterly journal of The Oceanography Society. Copyright 2018 by The Oceanography Society. All rights reserved.

## USAGE

Permission is granted to copy this article for use in teaching and research.

Republication, systematic reproduction, or collective redistribution of any portion of this article by photocopy machine, reposting, or other means is permitted only with the approval of The Oceanography Society. Send all correspondence to: [info@tos.org](mailto:info@tos.org) or The Oceanography Society, 1 Research Court, Suite 450, Rockville, MD 20850, USA.

# Steady Large-Scale Ocean Flows in Spherical Coordinates

By Adrian Constantin and Robin Stanley Johnson

**ABSTRACT.** We show that rotating spherical coordinates can and should be used for the study of steady, large-scale ocean flows, and describe the role of the stream function in simplifying the governing equations and for generating solutions.

## INTRODUCTION

Scientific advances typically evolve from the observation of natural phenomena, noting patterns and regularities; causal theories are then inferred. Such theories play an important role in the furtherance of knowledge by explaining the significance of what is already known and making predictions that might generate novel discoveries, which are subsequently subjected to experimental evaluation. Thus, scientific progress toward ever more accurate and comprehensive theories of nature occurs by experiment and observation, closely linked to theoretical developments.

To date, physical oceanography has been primarily an observational subject, and spectacular technological improvements have, in recent years, allowed the gathering of ocean data on a scale that would have been unimaginable to early scientists. Moreover, the computing power that is available now enables researchers to produce high-resolution numerical simulations of large-scale ocean models, and these can be compared with the wealth of available field data. However, we must be mindful that numerical solutions, no matter how accurate they may appear, suffer from discretization errors that naturally arise when a fluid continuum is represented numerically. Mathematics, on the other hand, is not merely useful in making specific observations intelligible, but it is instrumental in providing fundamental insights that are essential when we are attempting to understand the general motion of the ocean or trying to interpret numerical simulations. Indeed, ocean-data gathering is far from comprehensive and remains remarkably difficult, while numerical

simulations always involve some systematic errors, for example, due to the minimal spatial resolving power that is available. A feedback from the theoretical standpoint is essential if major failures in understanding are to be avoided, and to ameliorate the effects of systematic errors. Furthermore, while every location in the ocean is different, at least in some detail, it is important to move beyond regional features and aim to describe global ocean-flow characteristics that apply to long-duration features and change over fairly large (horizontal) distances (i.e., about 100 km and larger; see the discussion in Wunsch, 2015).

Earth is nearly an oblate spheroid (an ellipse rotated about its minor axis), with the equatorial bulge a consequence of the planet's rotation history. However, because no dynamical consequences of the small deviation from a perfect sphere—the polar radius being about 21 km shorter than the equatorial one (of length 6,378 km)—have been observed in ocean flows, a spherical Earth is an adequate model (see Wunsch, 2015). Depicting Earth as a sphere, and the fact that the ocean is a very thin layer on the spherical surface (with a mean thickness of about 0.1% of the radius: most oceanic depths are between 3 km and 5.5 km), has major consequences for the dynamics of ocean flows.

The inherent complexity of ocean flows, mainly due to the occurrence of nonlinear interactions on a wide array of spatial and temporal scales, precludes any attempt to solve the full governing equations with associated boundary and initial conditions. Thus, the challenge is to develop mathematically accurate and consistent approximate models for specific phenomena. Because every model omits some physical processes, but aims to identify the fundamental mechanisms on the relevant scales, it is essential to highlight overarching structural properties of these flows (e.g., conservation principles and quantities whose space-time evolution can be estimated with accuracy). In particular, large-scale ocean flows are affected by Earth's rotation

and, due to the associated Coriolis effect, the pattern that they exhibit is quite different from that of nonrotating fluids, and often they behave in ways that are counterintuitive. For example, if rotation is a dominant factor, then the water does not necessarily flow down a pressure gradient from high pressure to low-pressure regions; instead, it may circle around centers of high or low pressure. This type of behavior is observed in gyres—large-scale systems of circular ocean currents (see section on Gyre Visualization for more specific data)—driven and maintained by the ambient wind pattern and the forces created by Earth’s rotation. We believe that the investigation of nonlinear processes is of primary importance in developing a better understanding of the large-scale ocean circulation. Indeed, it is generally accepted that the nonlinear inertial terms are responsible for the formation and maintenance of gyre flows (see the discussion in Özkömen and Chassignet, 1998). Because of their size, any study of gyres must be based on the spherical geometry of Earth and the careful development of the resulting consequences. It is this aspect that will be the main thrust of the discussion presented in this paper. In particular, we will concentrate on the effective way to capture the main flow characteristics of gyres by means of stream functions in rotating spherical coordinates.

### GOVERNING EQUATIONS

Due to the fact that the magnitude of the vertical velocity component in a gyre is typically much smaller than the horizontal components (see Table 1), and that the ocean represents a thin layer on a rotating sphere, it is natural to model gyres as shallow water flows on a rotating sphere.

Table 1. Typical velocity components in a gyre.

DIRECTION	VALUE (IN M S <sup>-1</sup> )
Horizontal	10 <sup>-2</sup>
Vertical	10 <sup>-6</sup>

We introduce a set of (right-handed) spherical coordinates,  $(\varphi, \theta, r')$ :  $r'$  is the distance (radius) from the center of the sphere,  $\theta \in [-\pi/2, \pi/2]$  is the angle of latitude, and  $\varphi \in [0, 2\pi)$  is the azimuthal angle (i.e., the angle of longitude). (We use primes throughout the formulation of the problem to denote physical [dimensional] variables; these variables will be removed when we nondimensionalize.) The unit vectors in this  $(\varphi, \theta, r')$  system, for all points but the two poles, are  $(e_\varphi, e_\theta, e_r)$ , respectively, and we write the corresponding velocity components as  $(u', v', w')$ , with  $e_\varphi$  pointing from west to east,  $e_\theta$  from south to north, and  $e_r$  upward (see Figure 1); we avoid the poles because  $e_\varphi$  and  $e_\theta$  are not well defined there. The  $(\varphi, \theta, r')$  system is associated with a point fixed on the sphere that is rotating about its polar axis (with an angular speed  $\Omega' \approx 7.29 \times 10^{-5}$  rad s<sup>-1</sup>). The Navier-Stokes equation and the general equation of mass conservation are, respectively,

$$\begin{aligned} & \left( \frac{\partial}{\partial t'} + \frac{u'}{r' \cos \theta} \frac{\partial}{\partial \varphi} + \frac{v'}{r'} \frac{\partial}{\partial \theta} + w' \frac{\partial}{\partial r'} \right) (u', v', w') \\ & + \frac{1}{r'} (-u'v' \tan \theta + u'w', u'^2 \tan \theta + v'w', -u'^2 - v'^2) \\ & + 2\Omega' (-v' \sin \theta + w' \cos \theta, u' \sin \theta, -u' \cos \theta) \\ & + r' \Omega'^2 (0, \sin \theta \cos \theta, -\cos^2 \theta) \\ = & -\frac{1}{\rho'} \left( \frac{1}{r' \cos \theta} \frac{\partial p'}{\partial \varphi}, \frac{1}{r'} \frac{\partial p'}{\partial \theta}, \frac{\partial p'}{\partial r'} \right) + (0, 0, -g') \\ & + \nu'_1 \left( \frac{\partial^2}{\partial r'^2} + \frac{2}{r'} \frac{\partial}{\partial r'} \right) (u', v', w') \\ & + \frac{\nu'_2}{r'^2} \left( \frac{1}{\cos^2 \theta} \frac{\partial^2}{\partial \varphi^2} - \tan \theta \frac{\partial}{\partial \theta} + \frac{\partial^2}{\partial \theta^2} \right) (u', v', w'), \end{aligned}$$

and

$$\begin{aligned} & \frac{\partial \rho'}{\partial t'} + \frac{u'}{r' \cos \theta} \frac{\partial \rho'}{\partial \varphi} + \frac{v'}{r'} \frac{\partial \rho'}{\partial \theta} + w' \frac{\partial \rho'}{\partial r'} \\ & + \rho' \left\{ \frac{1}{r' \cos \theta} \frac{\partial u'}{\partial \varphi} + \frac{1}{r' \cos \theta} \frac{\partial}{\partial \theta} (v' \cos \theta) \right. \\ & \left. + \frac{1}{r'^2} \frac{\partial}{\partial r'} (r'^2 w') \right\} = 0, \end{aligned}$$

where  $p'(\varphi, \theta, r', t')$  is the pressure and  $\rho'(\varphi, \theta, r', t')$  the density, with  $g' = \text{constant} \approx 9.81 \text{ m s}^{-2}$ , a reasonable choice for the depths of the oceans on Earth. The coefficients of the viscous terms are constants:  $\nu'_1$  is the vertical kinematic eddy viscosity and  $\nu'_2$  is the horizontal kinematic eddy viscosity, with  $\nu'_2/\nu'_1$  typically of order  $10^3$  (see Talley et al., 2011). The viscous terms are only relevant in a boundary layer, within about 100 m from the surface, and if we are interested in the bulk motion, we simply set  $\nu'_1 \equiv 0$  and  $\nu'_2 \equiv 0$ , thus obtaining Euler’s equation in rotating spherical coordinates.

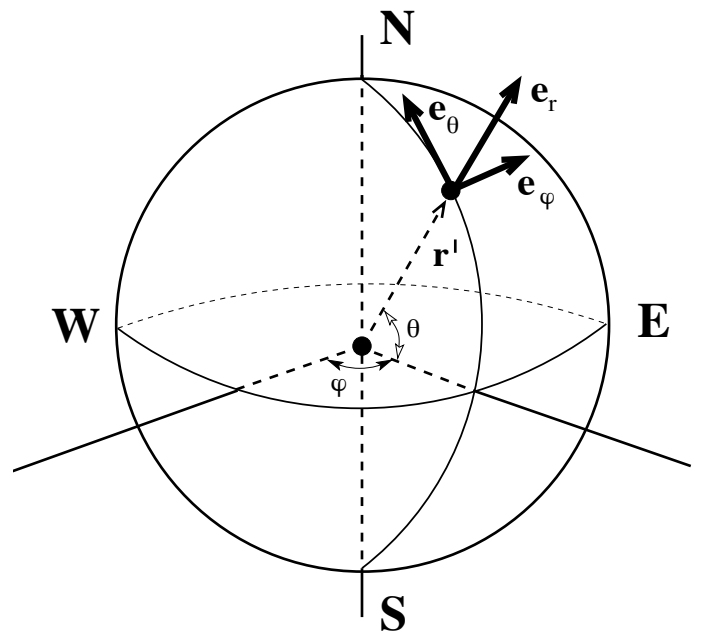


FIGURE 1. The rotating spherical coordinate system, where  $\theta$  is the angle of latitude,  $\varphi$  is the azimuthal angle, and  $r' = |r'|$  is the distance from the origin at Earth’s center. The North/South Poles are at  $\theta = \pm\pi/2$ , and the equator is on  $\theta = 0$ .

## GYRES AND SHALLOW-WATER FLOWS ON A ROTATING SPHERE

For large-scale motions in the near-surface ocean layer, which are affected by the movement of wind-driven surface waves, the frictional force is balanced by the Coriolis force, while friction is negligible at greater ocean depths. Thus, there are two aspects of gyre flows: the wind-induced currents in the surface boundary layer (where viscosity plays a dominant role), and the inviscid flow at greater depths. We will study both topics in the setting of constant density, following the recent approaches developed in Constantin and Johnson (2017b) and through more recent work of authors Constantin and Johnson.

### Ekman Layer

Under steady-state conditions, there is a balance between the Coriolis force and friction in the boundary layer of the upper ocean (of the order of 100 m). Let us first describe the boundary conditions that capture the dynamics of wind-induced currents. At the free surface,  $r' = R' + h'(\varphi, \theta)$ , where  $R' \approx 6,378$  km is the (mean) radius of Earth, we impose a surface pressure and the kinematic boundary condition:

$$p' = P'_s(\varphi, \theta) \quad \text{on} \quad r' = R' + h', \quad (1)$$

and

$$w' = \frac{u'}{r' \cos \theta} \frac{\partial h'}{\partial \varphi} + \frac{v'}{r'} \frac{\partial h'}{\partial \theta} \quad \text{on} \quad r' = R' + h', \quad (2)$$

respectively, where  $P'_s$  is the pressure at the surface. The velocity field should decay rapidly with depth in the near-surface layer, and we take the wind stress at the surface to be represented by

$$\frac{\partial u'}{\partial r'} = \tau'_1(\varphi, \theta), \quad \frac{\partial v'}{\partial r'} = \tau'_2(\varphi, \theta) \quad \text{on} \quad r' = R' + h'. \quad (3)$$

Redefining the pressure as

$$p' = \rho' \left( -g' r' + \frac{1}{2} r'^2 \Omega'^2 \cos^2 \theta \right) + P'(\varphi, \theta, r'), \quad (4)$$

and then writing  $r' = R' + z'$ , we nondimensionalize according to

$$z' = D' z, \quad (u', v', w') = U' (u, v, kw), \quad P' = \rho' U'^2 P,$$

where  $D'$  is the average depth of the surface layer,  $U'$  is a suitable speed scale (with  $0.1 \text{ m s}^{-1}$  typical for surface speeds in mid-latitudes) and the scaling factor  $k$  is yet to be chosen. On setting

$$\varepsilon = D'/R', \quad (5)$$

the governing equations (for steady flow in the surface layer  $-1 < z < 0$ ) become

$$\begin{aligned} & \left( \frac{u}{(1+\varepsilon z) \cos \theta} \frac{\partial}{\partial \varphi} + \frac{v}{1+\varepsilon z} \frac{\partial}{\partial \theta} + \frac{k}{\varepsilon} w \frac{\partial}{\partial z} \right) (u, v, kw) \\ & + \frac{1}{1+\varepsilon z} \left( -uv \tan \theta + kuw, u^2 \tan \theta + kvw, -u^2 - v^2 \right) \\ & + 2\omega (-v \sin \theta + kw \cos \theta, u \sin \theta, -u \cos \theta) \\ & = - \left( \frac{1}{(1+\varepsilon z) \cos \theta} \frac{\partial P}{\partial \varphi}, \frac{1}{1+\varepsilon z} \frac{\partial P}{\partial \theta}, \frac{1}{\varepsilon} \frac{\partial P}{\partial z} \right) \\ & + \frac{1}{R_{e1}} \left( \frac{1}{\varepsilon^2} \frac{\partial^2}{\partial z^2} + \frac{2}{(1+\varepsilon z)} \frac{1}{\varepsilon} \frac{\partial}{\partial z} \right) (u, v, kw) \\ & + \frac{1}{R_{e2}(1+\varepsilon z)^2} \left( \frac{1}{\cos^2 \theta} \frac{\partial^2}{\partial \varphi^2} - \tan \theta \frac{\partial}{\partial \theta} + \frac{\partial^2}{\partial \theta^2} \right) (u, v, kw); \end{aligned}$$

we have written

$$\omega = \Omega' R'/U', \quad R_{ei} = U' R'/\nu'_i \quad (i = 1, 2),$$

where  $\omega \approx 4,500$  (based on  $U' = 0.1 \text{ m s}^{-1}$ ), and  $R_{ei}$  denotes the appropriate Reynolds number. The equation of mass conservation becomes

$$\begin{aligned} & \frac{1}{(1+\varepsilon z) \cos \theta} \left[ \frac{\partial u}{\partial \varphi} + \frac{\partial}{\partial \theta} (v \cos \theta) \right] \\ & + \frac{k/\varepsilon}{(1+\varepsilon z)^2} \frac{\partial}{\partial z} \left[ (1+\varepsilon z)^2 w \right] = 0. \end{aligned}$$

The ratio of vertical speed to horizontal speed being typically smaller than  $10^{-4}$ , we set

$$k = \varepsilon \kappa,$$

where, for physically realistic solutions, we must have  $\kappa = O(1)$  or smaller; in this discussion, we consider  $\kappa = o(1)$ . We take the dominant viscous term to be that with the coefficient  $1/(\varepsilon^2 R_{e1})$ . This is accomplished by using this term as the basis for defining  $D'$ : write  $U' D' (D' = R')/\nu'_1 = 1$  and so

$$D' = \sqrt{R' \nu'_1 / U'}$$

(which gives, typically,  $\varepsilon \approx 10^{-5}$  and  $D' \approx 50 \text{ m}$ ). The horizontal eddy viscosity is now expressed as  $1/R_{e2} = \varepsilon^2 (\nu'_2 / \nu'_1) = \varepsilon^2 \mu$ , where  $\mu = \nu'_2 / \nu'_1$ . The nondimensional Navier-Stokes equation with all these choices (multiplying the third component throughout by  $\varepsilon$  and subsequently letting  $\varepsilon \rightarrow 0$ ) becomes at leading order

$$\begin{aligned} & \left( \frac{u}{\cos \theta} \frac{\partial}{\partial \varphi} + v \frac{\partial}{\partial \theta} \right) (u, v, 0) \\ & + (-uv \tan \theta, u^2 \tan \theta, 0) \\ & + 2\omega (-v \sin \theta, u \sin \theta, -u \cos \theta) \\ & = - \left( \frac{\partial P}{\partial \varphi}, \frac{\partial P}{\partial \theta}, \frac{\partial P}{\partial z} \right) + \frac{\partial^2}{\partial z^2} (u, v, 0). \end{aligned} \quad (6)$$

Correspondingly, at leading order the equation of mass conservation becomes

$$\frac{\partial u}{\partial \varphi} + \frac{\partial}{\partial \theta} (v \cos \theta) = 0. \quad (7)$$

The nondimensional versions of the boundary conditions follow directly, with the crucial requirement that the shear stresses at the surface must be present at leading order (so that the motion is wind-driven): on  $z = 0$  we specify

$$P = \bar{P}_s(\varphi, \theta), \quad \frac{\partial u}{\partial z} = \tau_1(\varphi, \theta), \quad \frac{\partial v}{\partial z} = \tau_2(\varphi, \theta), \quad (8)$$

coupled with the rapid decay with depth of the velocity within the surface layer  $-1 \leq z \leq 0$ .

### STREAM FUNCTION FORMULATION FOR MID-LATITUDE FLOWS

The vertical component of the velocity  $w$  is negligible at leading order (i.e.,  $\kappa = o(1)$ ), and at mid-latitudes, (7) implies the existence of a stream function  $\psi(\varphi, \theta, z)$  for the horizontal components of the velocity, with

$$u = -\psi_\theta, \quad v = \frac{1}{\cos \theta} \psi_\varphi. \quad (9)$$

Note that the particle paths of a steady flow at mid-latitudes on the sphere, with zonal velocity  $u$  and meridional velocity  $v$ , are along level sets of the stream function defined by (9) for fixed  $z$ . Indeed, if  $(\varphi(t), \theta(t))$  are the spherical coordinates (longitude and latitude, respectively) of a point

$$\mathfrak{P}(t) = \begin{pmatrix} \cos \theta(t) \cos \varphi(t) \\ \cos \theta(t) \sin \varphi(t) \\ \sin \theta(t) \end{pmatrix}$$

moving on the sphere centered at the origin and of unit radius such that it avoids the two poles, then the tangent vector

$$\mathfrak{P}' = \begin{pmatrix} -\theta' \sin \theta \cos \varphi - \varphi' \cos \theta \sin \varphi \\ -\theta' \sin \theta \sin \varphi + \varphi' \cos \theta \cos \varphi \\ \theta' \cos \theta \end{pmatrix}$$

has length  $\|\mathfrak{P}'\| = \sqrt{[\theta']^2 + [\varphi']^2 \cos^2(\theta)}$ . The computation of the unit tangent vector at the point  $(\varphi, \theta)$  for the flows  $s \mapsto (\varphi + s, \theta)$  and  $s \mapsto (\varphi, \theta + s)$  on the sphere yields

$$\mathbf{e}_\varphi = \begin{pmatrix} -\sin \varphi \\ \cos \varphi \\ 0 \end{pmatrix}, \quad \mathbf{e}_\theta = \begin{pmatrix} -\sin \theta \cos \varphi \\ -\sin \theta \sin \varphi \\ \cos \theta \end{pmatrix},$$

respectively. Therefore

$$u = \langle P', \mathbf{e}_\varphi \rangle = \varphi' \cos \theta, \quad v = \langle P', \mathbf{e}_\theta \rangle = \theta'.$$

Using (9), we see now that  $\partial_t \psi(\varphi(t), \theta(t), z) = 0$ , thus proving that the particle moves along a streamline.

In terms of the stream function, the elimination of the pressure in (6) gives the vorticity equation

$$\left( \psi_\varphi \frac{\partial}{\partial \theta} - \psi_\theta \frac{\partial}{\partial \varphi} \right) \left( \frac{1}{\cos^2 \theta} \psi_{\varphi\varphi} - \psi_\theta \tan \theta + \psi_{\theta\theta} + 2\omega \sin \theta \right) = \cos \theta \left( \frac{1}{\cos^2 \theta} \psi_{\varphi\varphi} - \psi_\theta \tan \theta + \psi_{\theta\theta} \right)_{zz}.$$

Mid-latitude flows in the Northern Hemisphere correspond to  $\theta \in (0, \pi/2)$ , and an exact solution is

$$\psi(\varphi, \theta, z) = \varphi F(z) - G(z) \ln(\cos \theta),$$

with  $F(z) = (1/2\omega)G''(z)$  for an arbitrary function  $G(z)$ . Here  $G(z)$  represents the relative vorticity (viewed in the rotating frame of reference), with the associated horizontal velocity field given by

$$u = G(z) \tan \theta, \quad v = -\frac{G''(z)}{2\omega \cos \theta}. \quad (10)$$

The total vorticity of the flow is obtained by adding to the relative vorticity the “spin vorticity,”  $2\omega \cos \theta$ , due to Earth’s rotation.

### LOCALIZED SOLUTIONS

To study in detail the flow pattern that has the leading order form derived in the section Stream Function Formulation for Mid-Latitude Flows, it is convenient to restrict our attention to an  $\varepsilon$ -neighborhood of a point  $(\varphi_0, \theta_0)$  on the surface of the sphere. While this procedure is analogous to the limitation to the  $f$ - or  $\beta$ -plane approximations, it captures more accurately (and consistently) the effects of spherical geometry. We set

$$\varphi = \varphi_0 + \varepsilon \Phi, \quad \theta = \theta_0 + \varepsilon \Theta, \quad P(\varphi, \theta, z) = \varepsilon \Pi(\Phi, \Theta, z),$$

and seek asymptotic solutions

$$\begin{aligned} u &\sim U_0(z) + \varepsilon u_1(\Phi, \Theta, z), \\ v &\sim V_0(z) + \varepsilon v_1(\Phi, \Theta, z), \\ w &\sim w_0(\Phi, \Theta, z) + \varepsilon w_1(\Phi, \Theta, z), \\ \Pi &\sim \Pi_0(\Phi, \Theta, z) + \varepsilon \Pi_1(\Phi, \Theta, z), \end{aligned}$$

with the choice of the leading order terms  $U_0$  and  $V_0$  based on (10) for a suitable  $G(z)$ , with the other functions determined at the next order. Following the recent work of authors Constantin and Johnson, we now discuss two relevant choices for the relative vorticity  $G(z)$ .

### 1. CLASSICAL EKMAN FLOW

For  $\theta \in (-\pi/2, \pi/2) \setminus \{0\}$  fixed and

$G(z) = \alpha_0 \cot \theta_0 e^{\lambda z} \cos(\lambda z + \chi)$  with  $\lambda = \sqrt{|\omega| \sin \theta_0}$  and  $\alpha_0, \chi$  arbitrary constants, we obtain the classical Ekman flow

$$\begin{cases} U_0(z) = \alpha_0 e^{\lambda z} \cos(\lambda z + \chi), \\ V_0(z) = \pm \alpha_0 e^{\lambda z} \sin(\lambda z + \chi), \end{cases} \quad (11)$$

with ordered signs: upper in the Northern Hemisphere and lower in the Southern Hemisphere. The key features of the horizontal velocity vector with the components (11) are that it spirals with increasing depth, decaying exponentially downward, and that the wind-induced surface current moves at an angle of  $\pi/4$  to the right/left of the wind in the Northern/Southern Hemisphere. The deflection angle can be inferred from (11) because the wind stress at the surface has the components

$$\tau_1 = \frac{\partial U_0}{\partial z}, \quad \tau_2 = \frac{\partial V_0}{\partial z} \quad \text{on } z = 0,$$

and therefore

$$U_0(0) + iV_0(0) = \frac{1}{\lambda\sqrt{2}} e^{\mp i\pi/4} [\tau_1 + i\tau_2]. \quad (12)$$

The Ekman layer depth  $D_E$  is the e-folding depth of the decaying horizontal velocity, that is, the distance over which it decreases by a factor of e. Its nondimensional value is  $1/\lambda$ , so that

$$D_E = \frac{1}{\lambda} D' = \sqrt{\frac{\nu'_1}{\Omega' |\sin \theta_0|}}.$$

With  $\nu'_1 = 0.05 \text{ m}^2 \text{ s}^{-1}$  for the typical mid-latitude vertical eddy viscosity (Talley et al., 2011), the Ekman depths at latitudes  $10^\circ$ ,  $45^\circ$ , and  $80^\circ$  are 63 m, 31 m, and 26 m, respectively. We should comment that, in some of the research literature, another definition of the Ekman depth is used: the depth at which the current (11) first moves in the opposite direction of the wind stress; due to (11)-(12), this depth is precisely  $3\pi/4 D_E$ , where  $3\pi/4 \approx 2.356$ . We also find the vertically integrated horizontal velocity component in the Ekman layer—the Ekman transport—in the form

$$\begin{cases} \overline{U}_0 = \int_{-1}^0 U_0(z) dz \approx \frac{\alpha_0}{2\lambda} (\cos \chi + \sin \chi), \\ \overline{V}_0 = \int_{-1}^0 V_0(z) dz \approx \mp \frac{\alpha_0}{2\lambda} (\cos \chi - \sin \chi), \end{cases}$$

invoking exponential decay with depth. Using (11)-(12), we can express the Ekman transport in terms of the wind stress:

$$\overline{U}_0 + i\overline{V}_0 = \frac{1}{2\lambda^2} e^{\mp i\pi/2} [\tau_1 + i\tau_2]. \quad (13)$$

We see that the Ekman transport is exactly perpendicular and to the right/left of the wind in the Northern/Southern Hemisphere. Ekman (1905) based his theoretical model on observations made by the Norwegian explorer Fridtjof Nansen, who in 1893 allowed his 39 m wooden ship *Fram* to be held frozen in the Arctic pack ice about 1,100 km south of the North Pole, thus hoping to drift with the ice and cross the North Pole. As *Fram* remained locked in pack ice and slowly drifted with it for 35 months, coming within 400 km of the North Pole, Nansen noticed that the direction of ice and ship movement was consistently between about  $20^\circ$  and  $40^\circ$  to the right of the prevailing wind direction. While Ekman's classical solution captures qualitatively the main features of wind-driven ocean currents (Rudnik, 2003), it exhibits noticeable quantitative mismatches. Addressing these could involve considering a depth-dependent eddy viscosity, which can accommodate deflection angles of the surface current that differ from  $45^\circ$ . However, the scarcity of explicit solutions for variable eddy viscosities (as well as the fact that the few at our disposal are not that transparent, being expressed in terms of special functions) requires heavy reliance on numerical simulations. An alternative approach was recently devised by authors Constantin and Johnson, based on an appropriate choice of the relative vorticity  $G(z)$  to generate suitable flows (10) at leading order.

## 2. EKMAN-TYPE FLOWS

For  $\theta \in (-\pi/2, \pi/2) \setminus \{0\}$  fixed and  $G(z) = \alpha_0 \cot \theta_0 e^{\lambda z} \cos(\chi + \delta \lambda z)$  with  $\alpha_0, \chi, \delta > 0, \lambda > 0$  constants, we obtain the Ekman-type flow

$$\begin{cases} U_0(z) = \alpha_0 e^{\lambda z} \cos(\chi + \delta \lambda z), \\ V_0(z) = \pm \frac{1}{2} \alpha_0 \lambda_0^2 (1 + \delta^2) e^{\lambda z} \sin(\chi - \chi_0 + \delta \lambda z), \end{cases}$$

with ordered signs (upper in the Northern Hemisphere and lower in the Southern Hemisphere), where  $\lambda = \lambda_0 \sqrt{|\omega| \sin \theta_0}$  and

$$\cos \chi_0 = \frac{2\delta}{1 + \delta^2}, \quad \sin \chi_0 = \frac{1 - \delta^2}{1 + \delta^2}.$$

Because

$$\begin{pmatrix} U_0(0) \\ V_0(0) \end{pmatrix} = \begin{pmatrix} \frac{2\lambda_0^2(3-\delta^2)}{4\lambda\lambda_0^2(1+\delta^2)} & \frac{\pm 4}{4\lambda\lambda_0^2(1+\delta^2)} \\ \frac{\mp \lambda_0^4(1+\delta^2)^2}{4\lambda\lambda_0^2(1+\delta^2)} & \frac{2\lambda_0^2(1+\delta^2)}{4\lambda\lambda_0^2(1+\delta^2)} \end{pmatrix} \begin{pmatrix} U'_0(0) \\ V'_0(0) \end{pmatrix},$$

we see that if the surface wind blows at the angle  $\beta$  relative to the eastward direction (measured in the usual counterclockwise sense, i.e.,  $\beta = \pi/2$  is to the north), then the angle for the direction of the surface current is

$$\gamma = \arctan \left( \frac{\mp \frac{1}{2} \lambda_0^4 (1 + \delta^2)^2 + \lambda_0^2 (1 + \delta^2) \tan \beta}{\lambda_0^2 (3 - \delta^2) \pm 2 \tan \beta} \right).$$

For  $\lambda_0 = \delta = 1$  we recover the classical Ekman flow but for  $\lambda_0 = 1$  and a wind blowing eastward ( $\beta = 0$ ), we find that  $\delta = 4/5$  gives a deflection angle of  $\gamma \approx 30^\circ$  to the right in the Northern Hemisphere, which has been observed in field data (see McWilliams and Huckle, 2006) and obtained in numerical simulations (see Zikanov et al., 2003). Note that the spiraling Ekman-type current turns at a rate slower than in Ekman's classical flow. Moreover, invoking the exponential decay, we compute the Ekman transport

$$\begin{aligned} \overline{U}_0 &= \int_{-1}^0 U_0(z) dz \approx \frac{\alpha_0 (\cos \chi + \delta \sin \chi)}{\lambda (1 + \delta^2)}, \\ \overline{V}_0 &= \int_{-1}^0 V_0(z) dz \approx \mp \frac{\alpha_0 \lambda_0^2 (\cos \chi - \delta \sin \chi)}{2\lambda}. \end{aligned}$$

Because

$$\begin{pmatrix} \overline{U}_0 \\ \overline{V}_0 \end{pmatrix} = \begin{pmatrix} \frac{4\lambda_0^2(1-\delta^2)}{2\lambda^2\lambda_0^2(1+\delta^2)} & \frac{\pm 4}{2\lambda^2\lambda_0^2(1+\delta^2)} \\ \frac{\mp \lambda_0^4(1+\delta^2)^2}{2\lambda^2\lambda_0^2(1+\delta^2)} & 0 \end{pmatrix} \begin{pmatrix} U'_0(0) \\ V'_0(0) \end{pmatrix},$$

we see that the angle of the mass transport vector  $(\overline{U}_0, \overline{V}_0)$  relative to the eastward direction is

$$\Gamma = \arctan \left( - \frac{\frac{1}{4} \lambda_0^4 (1 + \delta^2)^2}{\tan \beta \pm \lambda_0^2 (1 - \delta^2)} \right).$$

The classical Ekman result is recovered with the choice  $\lambda_0 = \delta = 1$  since in this case  $(\tan \Gamma)(\tan \beta) = -1$ . However, the generalized Ekman flow produces directions for the mass transport that differ from the usual  $90^\circ$ ; in the example used above (Northern Hemisphere,  $\beta = 0, \lambda_0 = 1, \delta = 4/5$ ), we find that the angle is about  $62^\circ$  (to the right; see Figure 2).

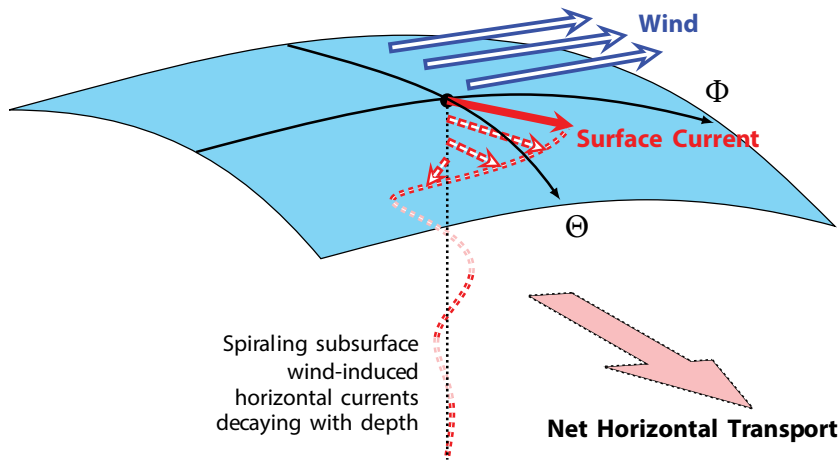


**FIGURE 2.** Sketch of the near-surface horizontal currents driven by a steady eastward wind in the Northern Hemisphere: the surface current is deflected at an angle of about  $30^\circ$  to the right of the wind direction, while beneath the surface the velocity direction rotates to the right of that in the layer above, producing a spiraling current whose speed rapidly decays as the depth increases, with a net water transport about  $62^\circ$  to the right of the wind direction.

### Inviscid Mid-Latitude Flows

The study of large-scale ocean circulation, with no wind input and no friction, was pioneered by Fofonoff (1954), but these initial investigations relied on the  $\beta$ -plane approximation, which treats an ocean region as being locally flat in all respects except in the latitudinal variation in the Coriolis parameter. The study of large-scale inviscid flows in rotating spherical coordinates was initiated recently in Constantin and Johnson (2017b). The importance of the need to use the full structure of spherical geometry is evident when we note that, in non-equatorial regions, the  $\beta$ -plane approximation leads to inconsistencies (see the discussion in Dellar, 2011). On the other hand, gyre flows are not encountered in equatorial ocean regions because the vanishing of the meridional component of the Coriolis force at the equator results in the equator acting as a fictitious natural boundary, facilitating azimuthal flow propagation; for a discussion of equatorial currents, which typically present an elaborate vertical structure, we refer to Johnson et al. (2001) for data, and to Constantin and Johnson (2016, 2017a) for theoretical studies. Moreover, although waves play an insignificant role on the scales that are appropriate for gyres, they are important ingredients in wave-current interactions for equatorial flows (see Constantin, 2012; Constantin and Johnson, 2015; Henry, 2016).

The governing equations for inviscid flow are those from the section above on Governing Equations, with  $v'_1 = 0$  and  $v'_2 = 0$ , with the boundary condition (3) ignored and the rapid decay of the velocity field in the near-surface layer replaced by the requirement that, at the bottom of the ocean,  $r' = R' + d'(\varphi, \theta)$ , which we take to be an impermeable, solid boundary, we have the kinematic boundary condition

$$w' = \frac{u'}{r' \sin \theta} \frac{\partial d'}{\partial \varphi} + \frac{v'}{r'} \frac{\partial d'}{\partial \theta} \quad \text{on} \quad r' = R' + d'(\varphi, \theta).$$

We nondimensionalize according to

$$z' = H'z, \quad (u', v', w') = U'(u, v, kw), \quad P' = \rho'U'^2P,$$

where  $H'$  is the average depth of the ocean and  $U' = \sqrt{H'g'}$  and the scaling factor  $k$  associated with the vertical component of the velocity is yet to be chosen. We set

$$\varepsilon = \frac{H'}{R'}, \quad \omega = \frac{\Omega'R'}{U'}, \quad P = \Pi + \frac{\omega^2}{4} \cos(2\theta),$$

and then a suitable choice of scaling for the vertical velocity component is  $k = \varepsilon^2$ : this satisfies  $k = o(\varepsilon)$  and leads to a particularly simple asymptotic structure for the solution, based on the sequence  $\{e^n\}_{n \geq 0}$ . The leading-order problem then becomes

$$\left\{ \begin{array}{l} \frac{\partial \Pi}{\partial z} = 0, \\ \left( \frac{u}{\cos \theta} \frac{\partial}{\partial \varphi} + v \frac{\partial}{\partial \theta} \right) (u, v, 0) \\ \quad + \left( -uv \tan \theta, u^2 \tan \theta, 0 \right) \\ \quad + 2\omega (-v \sin \theta \cos \theta, u \sin \theta, 0) \\ \\ = - \left( \frac{1}{\sin \theta} \frac{\partial \Pi}{\partial \varphi}, \frac{\partial \Pi}{\partial \theta}, 0 \right), \\ \frac{\partial u}{\partial \varphi} + \frac{\partial}{\partial \theta} (v \cos \theta) = 0, \end{array} \right. \quad (14)$$

the appropriate boundary condition at this order being

$$\Pi = P_s(\theta, \varphi) + \frac{\omega^2}{4} \cos(2\theta) \quad \text{on} \quad z = 0, \quad (15)$$

with the condition on the bottom automatically satisfied with  $d(\varphi, \theta) = \text{constant}$ , which is a reasonable assumption (though this choice of  $d$  is not a necessary requirement). The last equation in (14) permits us to introduce a stream function  $\psi(\varphi, \theta)$ , defined up to an additive constant by (9), and the compatibility condition generated by the elimination of  $\Pi$  in (14) produces the vorticity equation

$$\left( \psi_\varphi \frac{\partial}{\partial \theta} - \psi_\theta \frac{\partial}{\partial \varphi} \right) \left( \frac{1}{\cos^2 \theta} \psi_{\varphi\varphi} - \psi_\theta \tan \theta \right. \\ \left. + \psi_{\theta\theta} + 2\omega \sin \theta \right) = 0. \quad (16)$$

Here, the vorticity in the flow, at leading order, expressed in spherical coordinates, is

$$\nabla^2 \psi = \frac{1}{\cos^2 \theta} \psi_{\varphi\varphi} - \psi_{\theta} \tan \theta + \psi_{\theta\theta}. \quad (17)$$

Introducing the relative vorticity (relative to Earth's surface and not driven by Earth's rotation)

$$\Psi(\varphi, \theta) = \psi(\varphi, \theta) + \omega \sin \theta,$$

the vorticity equation (16) becomes

$$\left( (\Psi - \omega \sin \theta)_{\varphi} \frac{\partial}{\partial \theta} - (\Psi - \omega \sin \theta)_{\theta} \frac{\partial}{\partial \varphi} \right) \left( \frac{1}{\cos^2 \theta} \Psi_{\varphi\varphi} - \Psi_{\theta} \tan \theta + \Psi_{\theta\theta} \right) = 0. \quad (18)$$

Throughout regions where  $\nabla_{(\varphi, \theta)}(\Psi - \omega \sin \theta) \neq (0, 0)$ , the rank theorem (Newns, 1967) permits us to express the total vorticity of the solution of (18) in the form  $F(\Psi - \omega \sin \theta) + 2\omega \sin \theta$ , so that

$$\frac{1}{\cos^2 \theta} \Psi_{\varphi\varphi} - \Psi_{\theta} \tan \theta + \Psi_{\theta\theta} = F(\Psi - \omega \sin \theta) \quad (19)$$

for an arbitrary function  $F$ . However, if  $F(a) \neq 0$ , then this variant of the vorticity equation (19), does not capture the simple explicit solutions

$$\Psi = \omega \sin \theta + a$$

of (18), representing stationary flows  $\psi = a$ , where  $a$  is an arbitrary constant. We also note that the classical form of the vorticity equation (in planar geometry) is  $\Delta \Psi = F(\Psi)$ ; see Andreev et al. (1998) for a systematic analysis of its exact solutions and for their graphical illustration.

Classes of explicit solutions of (19) were obtained in Constantin and Johnson (2017b). These rely on the observation that, while the vorticity inherent in the motion of the ocean is expected to be significantly larger than that provided by Earth's rotation, there is no coupling in the case of constant oceanic vorticity. However, we will see that coupling necessarily occurs even in the case of functions  $F$  that are linear in their arguments.

### 1. ZERO OCEANIC VORTICITY

In the case  $F = 0$  we have the solution

$$\Psi = \alpha \ln \left\{ \varphi^2 + \left[ A + \ln \left( \tan \left( \frac{\cos \theta}{1 - \sin \theta} \right) \right) \right]^2 \right\},$$

where  $\alpha$  and  $A$  are arbitrary constants; this expression corresponds precisely with the classical solution for irrotational flow in two-dimensional, planar geometry.

### 2. CONSTANT NON-ZERO OCEANIC VORTICITY

For constant vorticity ( $F = \gamma$ ), a solution of (19) is

$$\Psi = \frac{\gamma}{\beta} \left\{ \varphi^2 - \left[ A + \ln \left( \frac{\cos \theta}{1 - \sin \theta} \right) \right]^2 - \beta \ln \cos \theta \right\},$$

to within an additive constant; the strength of the velocity field is now proportional to  $\gamma/\beta$ , and the choice of  $\beta$  (for a given constant vorticity  $\gamma$ ) controls the type of solutions available. The

streamlines for the choice  $A = -0.4$  and  $\beta = 4$  are depicted in Figure 3, with the value of  $\gamma \neq 0$  irrelevant in these plots since it simply measures the magnitude of the velocity field.

### 3. ZERO TOTAL VORTICITY

For  $F(\zeta) = 2\omega \tanh(\frac{2\zeta}{\omega})$ , the solution

$$\Psi(\theta) = \omega \sin \theta - \frac{\omega}{2} \tanh^{-1}(\sin \theta)$$

of the equation  $F(\Psi - \omega \sin \theta) = -2\omega \sin \theta$  ensures that the total vorticity is zero.

### 4. COUPLING BETWEEN THE OCEANIC FLOW AND THE FLOW DRIVEN BY EARTH'S ROTATION

In the case when the function  $F$  is linear and homogeneous, (19) takes on the form

$$\frac{1}{\cos^2 \theta} \Psi_{\varphi\varphi} - \Psi_{\theta} \tan \theta + \Psi_{\theta\theta} = \lambda(\Psi - \omega \sin \theta),$$

for some constant  $\lambda$ . This equation can be solved using spherical harmonic functions. Note that a particular solution of this equation is

$$\Psi = \frac{\lambda\omega}{\lambda + 2} \cos \theta,$$

and so there exists a solution of the homogeneous equation (for  $\lambda = -2$ ), which is resonant with this particular rotation-driven solution.

### GYRE VISUALIZATION

The understanding of physical phenomena is considerably helped by visual representations that can illuminate both qualitative and quantitative aspects. Of course, it is impossible to perform geophysical experiments on planetary scales, and laboratory experiments often present considerable deviations from

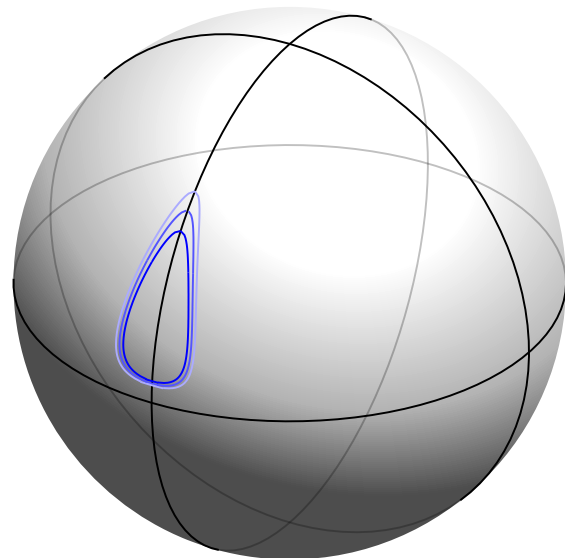
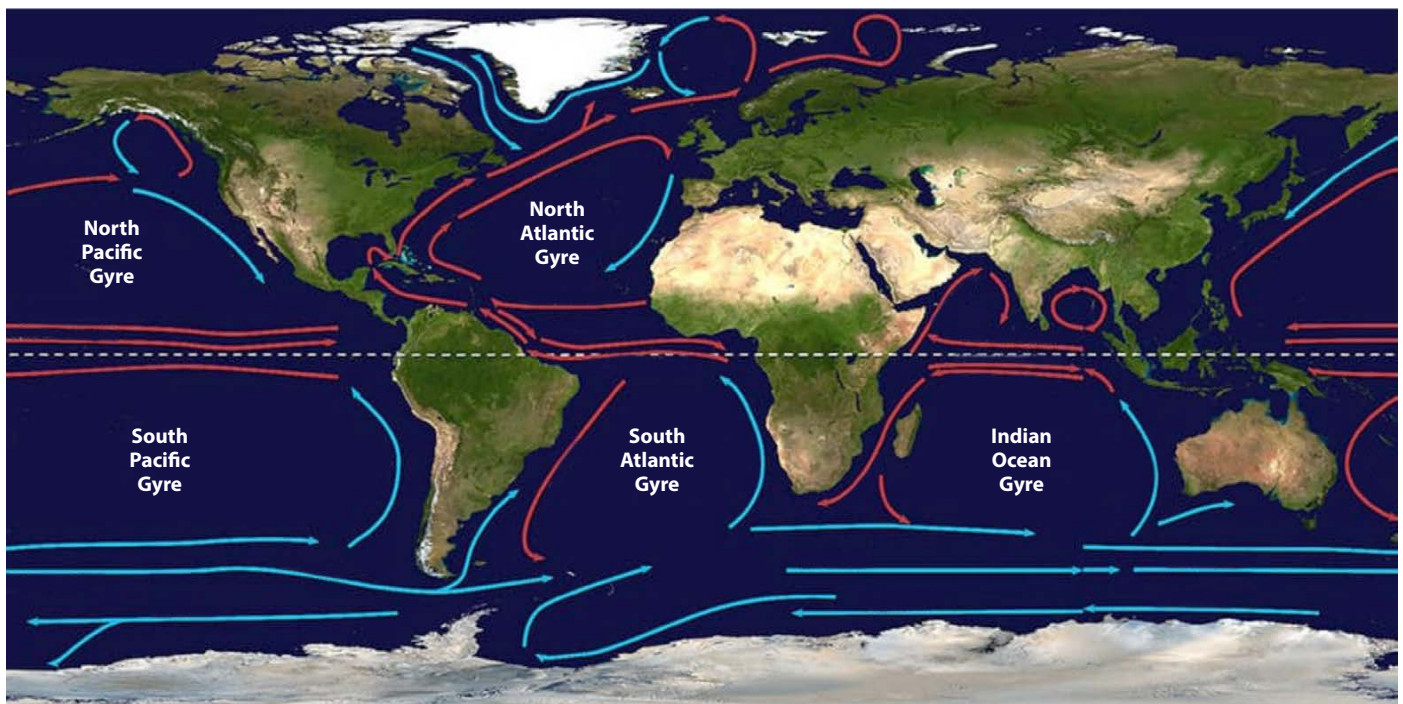


FIGURE 3. Depiction of three closed streamlines for a gyre flow with constant non-zero relative vorticity at mid-latitudes in the Northern Hemisphere.



**FIGURE 4.** The most significant ocean currents (warm currents shown in red and cold currents in blue), some of which make up the five major ocean-wide gyres. These large systems of circular ocean currents are driven by the interaction of global wind patterns and the Coriolis force, which is due to Earth's rotation. The largest ocean gyre is the North Pacific Gyre, comprising about 20 million square kilometers. Current speeds within gyres vary considerably, the swiftest currents being the northeastward flowing Gulf Stream of the northwestern Atlantic and the Kuroshio of the northwestern Pacific, with velocities averaging  $1 \text{ m s}^{-1}$  and peaking at about  $2 \text{ m s}^{-1}$ , while the maximal speed of eastern boundary currents is in the range  $5\text{--}15 \text{ cm s}^{-1}$ . Image credit: NOAA

real-world dynamical behavior. In addition to their scientific interest, fluid flow images often have an aesthetic appeal.

There are large-scale polar gyres: the ice-covered Beaufort gyre in the Arctic Ocean (approximately 1,500 km across, making one complete rotation about every four years, with typical speeds of about  $1 \text{ cm s}^{-1}$ ) and the Weddell and Ross gyres in the Southern Ocean (having diameters of the order of 2,000 km and surface speeds peaking at about  $10 \text{ cm s}^{-1}$ , both with seasonal ice covers). However, the five largest ocean gyres are subtropical: the North and South Pacific Gyres, the North and South Atlantic Gyres, and the Indian Ocean Gyre (see Figure 4). In addition, gyres are encountered in other oceanic regions (see Figure 5) but never at the equator (where the Coriolis effect is nonexistent, thus inhibiting the deflection of ocean currents that propagate in equatorial regions predominantly along the east-west direction). Most gyres are stable but some do experience seasonal variations; for example, the small-scale but energetic Ierapetra gyre (having a diameter of about 100–300 km and featuring surface horizontal velocities reaching  $5 \text{ cm s}^{-1}$ ) shows up southeast of Crete, in the Eastern Mediterranean, at the end of summer almost every year (see Amitai et al., 2010; Poulain et al., 2012).

It is worth emphasizing that a better understanding of ocean gyres provides clues that contribute to the study of atmospheric flows on other planets. For example, Saturn is one of our solar system's quartet of gas giants (together with Jupiter, Uranus, and Neptune), and its atmosphere (consisting of about 75%

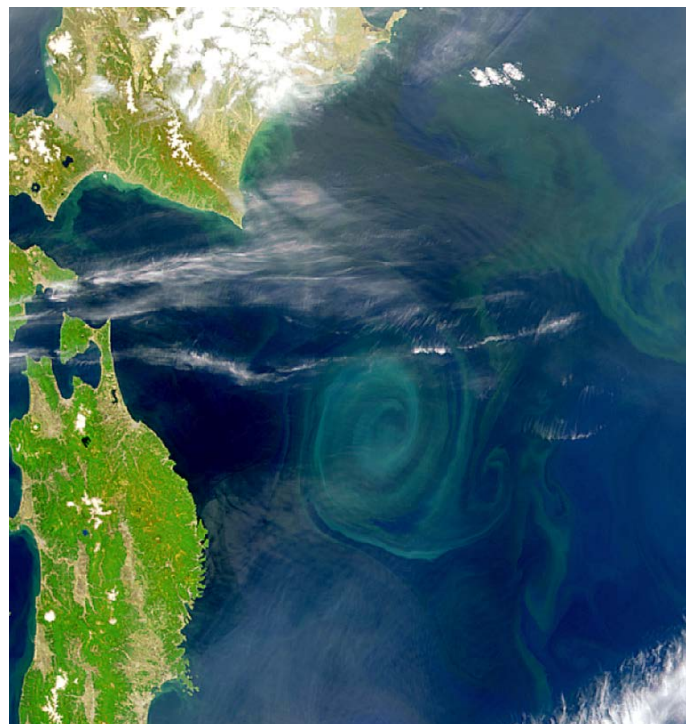


**FIGURE 5.** Satellite image of a recirculation gyre in the North Pacific, east of the coast of Japan, created by the collision of the warm northward Kuroshio current with the cold subarctic Kurile current near Hokkaido. Phytoplankton growing in the surface waters provide the milky green color that trace out the circular gyre flow. Image credit: SeaWiFS Project, NASA/Goddard Space Flight Center, and ORBIMAGE

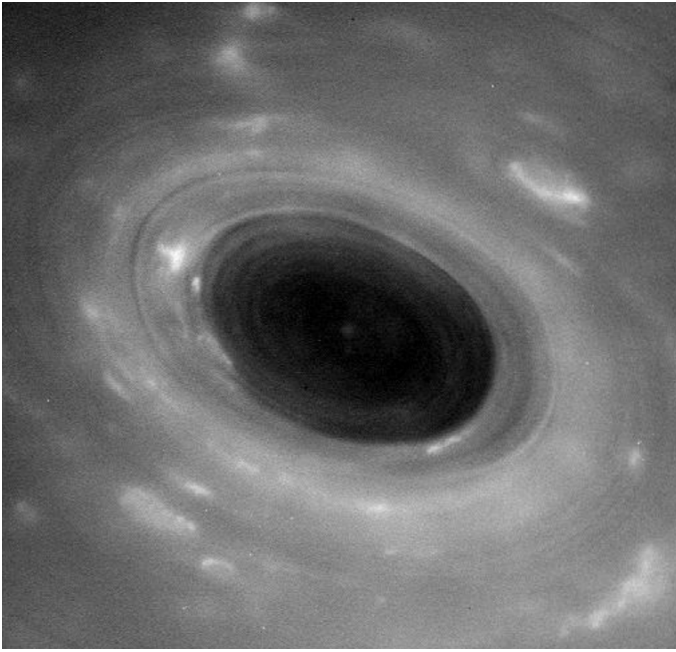


**FIGURE 6.** Photo of the spinning gyre centered at Saturn's North Pole, with a radius of about 945 km (out to 88.5°N) and wind speeds of 150 m s<sup>-1</sup>, captured by the NASA's Cassini spacecraft in 2017. Image credit: NASA/JPL-Caltech/Space Science Institute

hydrogen and 25% helium, with traces of other gases such as methane) features a huge gyre centered at the planet's north pole (see Figure 6). While there is some ongoing scientific debate about the exact source of the gyre's motion, there is no doubt that the planet's rotation about its polar axis and the stratification of its atmosphere are both key elements in its maintenance. Thermal images indicate that, while the gyre reaches roughly 100 km down into Saturn's atmosphere, its motion is predominantly horizontal. The similarity to ocean gyres is underlined by the fact that recent simulations of Saturn's north pole gyre are based on the presumed relevance of shallow-water models to this astrophysical flow (see O'Neill et al., 2015). 

## REFERENCES

Amitai, Y., Y. Lehahn, A. Lazar, and E. Heifetz. 2010. Surface circulation of the eastern Mediterranean Levantine basin: Insights from analyzing 14 years of satellite altimetry data. *Journal of Geophysical Research* 115(C10), <https://doi.org/10.1029/2010JC006147>.

Andreev, V.K., O.V. Kaptsov, V.V. Pukhnachev, and A.A. Rodionov. 1998. *Applications of Group-Theoretical Methods in Hydrodynamics*. Kluwer Academic Publishers, Dordrecht, 396 pp., <https://doi.org/10.1007/978-94-017-0745-9>.

Constantin, A. 2012. An exact solution for equatorially trapped waves. *Journal of Geophysical Research* 117, C05029, <https://doi.org/10.1029/2012JC007879>.

Constantin, A., and R.S. Johnson. 2015. The dynamics of waves interacting with the Equatorial Undercurrent. *Geophysical & Astrophysical Fluid Dynamics* 109:311–358, <https://doi.org/10.1080/03091929.2015.1066785>.

Constantin, A., and R.S. Johnson. 2016. An exact, steady, purely azimuthal equatorial flow with a free surface. *Journal of Physical Oceanography* 46:1,935–1,945, <https://doi.org/10.1175/JPO-D-15-0205.1>.

Constantin, A., and R.S. Johnson. 2017a. A nonlinear, three-dimensional model for ocean flows, motivated by some observations of the Pacific equatorial undercurrent and thermocline. *Physics of Fluids* 29, 056604, <https://doi.org/10.1063/1.4984001>.

Constantin, A., and R.S. Johnson. 2017b. Large gyres as a shallow-water asymptotic solution of Euler's equation in spherical coordinates. *Proceedings of the Royal Society A* 473(2200), <https://doi.org/10.1098/rspa.2017.0063>.

Dellar, P.J. 2011. Variations on a beta-plane: Derivation of non-traditional beta-plane equations from Hamilton's principle on a sphere. *Journal of Fluid Mechanics* 674:174–195, <https://doi.org/10.1017/S0022212010006464>.

Ekman, V.W. 1905. On the influence of the Earth's rotation on ocean currents. *Arkiv för matematik, astronomi och fysik* 2:1–52.

Fofonoff, N.P. 1954. Steady flow in a frictionless homogeneous ocean. *Journal of Marine Research* 13:254–262.

Henry, D. 2016. Equatorially trapped nonlinear water waves in a  $\beta$ -plane approximation with centripetal forces. *Journal of Fluid Mechanics* 804, R1, <https://doi.org/10.1017/jfm.2016.544>.

Johnson, G.C., M.J. McPhaden, and E. Firing. 2001. Equatorial Pacific Ocean horizontal velocity, divergence, and upwelling. *Journal of Physical Oceanography* 31(3):839–849, [https://doi.org/10.1175/1520-0485\(2001\)031<0839:EPOHVD>2.0.CO;2](https://doi.org/10.1175/1520-0485(2001)031<0839:EPOHVD>2.0.CO;2).

McWilliams, J.C., and E. Huckle. 2006. Ekman layer rectification. *Journal of Physical Oceanography* 36:1,646–1,659, <https://doi.org/10.1175/JPO2912.1>.

Newns, W.F. 1967. Functional dependence. *The American Mathematical Monthly* 74:911–920, <https://doi.org/10.2307/2315264>.

O'Neill, M.E., K.E. Emanuel, and G.R. Flierl. 2015. Polar vortex formation in giant-planet atmospheres due to moist convection. *Nature Geoscience* 8:523–527, <https://doi.org/10.1038/ngeo2459>.

Özkoimen, T.M., and E.C. Chassignet. 1998. Emergence of inertial gyres in a two-layer quasigeostrophic ocean model. *Journal of Physical Oceanography* 28:461–484, [https://doi.org/10.1175/1520-0485\(1998\)028<0461:EOIGIA>2.0.CO;2](https://doi.org/10.1175/1520-0485(1998)028<0461:EOIGIA>2.0.CO;2).

Poulain, P.-M., M. Menna, and E. Mauri. 2012. Surface geostrophic circulation of the Mediterranean Sea derived from drifter and satellite altimeter data. *Journal of Physical Oceanography* 42:973–990, <https://doi.org/10.1175/JPO-D-11-0159.1>.

Rudnik, D.L. 2003. Observations of momentum transfer in the upper ocean: Did Ekman get it right? Pp. 163–170 in *Near-Boundary Processes and Their Parameterization: Proceedings of the 13th Aha Huliko'a Winter Workshop*. University of Hawaii at Manoa, Honolulu, HI.

Talley, L.D., G.L. Pickard, W.J. Emery, and J.H. Swift. 2011. *Descriptive Physical Oceanography: An Introduction*. Academic Press, 560 pp.

Wunsch, C. 2015. *Modern Observational Physical Oceanography*. Princeton University Press, New Jersey, 512 pp.

Zikanov, O., D.N. Slinn, and M.R. Dhanak. 2003. Large eddy simulations of the wind-induced turbulent Ekman layer. *Journal of Fluid Mechanics* 495:343–368, <https://doi.org/10.1017/S0022212003006244>.

## ACKNOWLEDGMENTS

This research was supported by Vienna Science and Technology Fund research grant MA16-009. The authors are grateful for helpful comments from the referees.

## AUTHORS

**Adrian Constantin** (adrian.constantin@univie.ac.at) is Professor of Mathematics, University of Vienna, Austria. **Robin Stanley Johnson** (r.s.johnson@ncl.ac.uk) is Professor Emeritus of Applied Mathematics, University of Newcastle upon Tyne, United Kingdom.

## ARTICLE CITATION

Constantin, A., and R.S. Johnson. 2018. Steady large-scale ocean flows in spherical coordinates. *Oceanography* 31(3):42–50, <https://doi.org/10.5670/oceanog.2018.308>.